

Trace finite element method for the surface (Navier–)Stokes problem

Alexander Zhiliakov*

October 21, 2019

Contents

1	Navier–Stokes problem on the evolving surface	2
1.1	Continuous problem and operator splitting	2
1.2	Tangential component equation	2
1.2.1	Discretization	2
1.2.2	Numerical experiments	3
1.3	Normal component equation	3
2	Preliminaries	4
2.1	Bilinear forms and matrices	4
2.2	Quadratures for bilinear forms	5
2.3	Error computation	8
3	Convergence results	8
3.1	Manufactured solution	8
3.2	$P_2 - P_1$ Trace FEM	10
3.2.1	Inconsistent penalty formulation	10
3.2.2	Consistent penalty formulation	11
4	Inf-sup stability: pressure Schur complement generalized eigenvalues	13
4.1	Solution description	13
4.2	Dependency of the spectrum on the mesh size	14
4.3	Sensitivity of the spectrum to levelset shifts	16
5	Notes on DROPS implementation	17
5.1	VTK output	17

*Department of Mathematics, University of Houston, Houston, Texas 77204 (alex@math.uh.edu).

1 Navier–Stokes problem on the evolving surface

1.1 Continuous problem and operator splitting. We consider surface Navier–Stokes equations for inextensible viscous material surface $\Gamma = \Gamma(t)$

$$\begin{aligned} \frac{d\mathbf{u}}{dt} - \nu \operatorname{div}_\Gamma(E_s(\mathbf{u})) + \nabla_\Gamma p - p \kappa \mathbf{n} &= \mathbf{f}, \\ \operatorname{div}_\Gamma \mathbf{u} &= g \end{aligned} \tag{1}$$

with d/dt denoting material (full) derivative operator, cf. [3, p. 8]. As standard in the analysis of the Navier–Stokes equations, we introduced dimensionless variables in (1) so that $\|\mathbf{u}\|_{L^\infty(\Gamma)} = 1$, with Reynolds number ν^{-1} .

Performing operator splitting technique, one may rewrite system (1) as two systems: One for the tangential, and another one for the normal component of the velocity field $\mathbf{u} = \mathbf{u}_T + u_N \mathbf{n}$. Namely,

$$\begin{aligned} \mathbf{P} \frac{d\mathbf{u}_T}{dt} - \nu \mathbf{P} \operatorname{div}_\Gamma(E_s(\mathbf{u}_T)) + u_N \mathbf{H} \mathbf{u}_T + \nabla_\Gamma p &= \mathbf{f}_T + \nu \mathbf{P} \operatorname{div}_\Gamma(u_N \mathbf{H}) + u_N \nabla_\Gamma u_N, \\ \operatorname{div}_\Gamma \mathbf{u}_T &= g - u_N \kappa \end{aligned} \tag{2}$$

and

$$\frac{du_N}{dt} = \nu \mathbf{n} \cdot \operatorname{div}_\Gamma(E_s(\mathbf{u})) + p \kappa + f_N + D \mathbf{n} \cdot \mathbf{u}_T. \tag{3}$$

Note that systems (2) and (3) are coupled. **AZ: TODO:** Rewrite (3) similar to (2), i.e. in such a form so that the left-hand side **only** has terms dependent on u_N , and all the rest goes to the right-hand side.

The normal component of the velocity defines surface dynamics. Thus the level-set function ϕ satisfies the transport equation

$$\frac{d\phi}{dt} := \frac{\partial\phi}{\partial t} + u_N \mathbf{n} \cdot \nabla \phi = 0. \tag{4}$$

1.2 Tangential component equation. Our numerical scheme will be based on the operator splitting introduced above. For the time being, let us assume that the surface dynamics is defined: ϕ is given, and then from (4) we have $u_N = -\frac{\partial\phi}{\partial t} / \|\nabla\phi\|$. Then we rewrite (2) as

$$\begin{aligned} \frac{\partial \mathbf{u}_T}{\partial t} + \mathbf{P}(\mathbf{u} \cdot \nabla) \mathbf{u}_T - \nu \mathbf{P} \operatorname{div}_\Gamma(E_s(\mathbf{u}_T)) + u_N \mathbf{H} \mathbf{u}_T + \nabla_\Gamma p &= \mathbf{f}_T, \\ \operatorname{div}_\Gamma \mathbf{u}_T &= g, \end{aligned} \tag{5}$$

where for the sake of simplicity we kept the same notation for the given right-hand side data (i.e. we set $g \stackrel{(2)}{=} g - u_N \kappa$ and similar for \mathbf{f}_T).

1.2.1 Discretization. We start with the time discretization. Consider the time frame $t_i := i \Delta t$. Approximating the time derivative with some finite difference and linearizing the convective term via extrapolation of the wind field from previous time frames $t_{j < i}$, we arrive at the following Oseen-type problem posed on the stationary surface $\Gamma(t_i)$: Find (\mathbf{u}_T, p) such that

$$\begin{aligned} \alpha \mathbf{u}_T + \mathbf{P}(\mathbf{w} \cdot \nabla) \mathbf{u}_T - \nu \mathbf{P} \operatorname{div}_\Gamma(E_s(\mathbf{u}_T)) + \beta \mathbf{H} \mathbf{u}_T + \nabla_\Gamma p &= \mathbf{f}_T, \\ \operatorname{div}_\Gamma \mathbf{u}_T &= g \end{aligned} \tag{6}$$

with $g \stackrel{(5)}{=} g(\cdot, t_i)$ and $\beta \stackrel{(5)}{=} u_N(\cdot, t_i)$. The solution (\mathbf{u}_T, p) of (6) approximates the solution of (5) at time $t = t_i$.

- At the first time frame $i = 1$ we utilize backward Euler approximation for the time derivative and initial data $\mathbf{u}^0 := \mathbf{u}(\cdot, 0)$ for the wind field \mathbf{w} . Thus we have

$$\alpha := \Delta t^{-1}, \quad \mathbf{w} := \mathbf{u}^0, \quad \mathbf{f}_T := \mathbf{f}_T^i + \Delta t^{-1} \mathbf{u}_T^0,$$

- At time frames $i > 1$ we utilize BDF2 approximation for the time derivative and linear extrapolation for the wind field \mathbf{w} . Denoting the (approximate) velocity solution at time $t = t_j$ by \mathbf{u}^j , we have

$$\alpha := \frac{3}{2} \Delta t^{-1}, \quad \mathbf{w} := 2 \mathbf{u}^{i-1} - \mathbf{u}^{i-2}, \quad \mathbf{f}_T := \mathbf{f}_T^i + 2 \Delta t^{-1} \mathbf{u}_T^{i-1} - \frac{1}{2} \Delta t^{-1} \mathbf{u}_T^{i-2},$$

This results in a semi-implicit time scheme.

Next we consider the weak formulation for (6): Find $(\mathbf{u}_T, p) \in \mathbf{V}_T \times Q$ s.t.

$$\begin{aligned} a(\mathbf{u}_T, \mathbf{v}_T) + b_T(\mathbf{v}_T, q) &= (\mathbf{f}_T, \mathbf{v}_T), \\ -b_T(\mathbf{u}_T, q) &= (g, q) \end{aligned} \tag{7}$$

holds for all $(\mathbf{v}_T, q) \in \mathbf{V}_T \times Q$. **AZ: TODO: Add definitions of forms and spaces.** In order to deal with the dominating convection case, $\nu \ll 1$, we regularize (7) via introducing augmented Lagrangian / grad-div type stabilization [1]. Choosing test function $q = \operatorname{div}_\Gamma \mathbf{v}_T = \operatorname{tr} E_s(\mathbf{v}_T)$ in the second equation of (7) and adding it to the first one, we end up with

$$\underbrace{a(\mathbf{u}_T, \mathbf{v}_T) + \gamma (\operatorname{tr} E_s(\mathbf{u}_T), \operatorname{tr} E_s(\mathbf{v}_T))}_{a_\gamma(\mathbf{u}_T, \mathbf{v}_T)} + b(\mathbf{v}_T, q) = (\mathbf{f}_T, \mathbf{v}_T) + \gamma (g, \operatorname{tr} E_s(\mathbf{v}_T)) =: (\mathbf{f}_\gamma, \mathbf{v}_T),$$

where we introduced an augmented bilinear form $a_\gamma(\cdot, \cdot)$ and linear functional $(\mathbf{f}_\gamma, \cdot)$ with a regularization parameter $\gamma \geq 0$. Thus our regularized weak problem reads as

$$\begin{aligned} a_\gamma(\mathbf{u}_T, \mathbf{v}_T) + b_T(\mathbf{v}_T, q) &= (\mathbf{f}_\gamma, \mathbf{v}_T), \\ -b_T(\mathbf{u}_T, q) &= (g, q). \end{aligned} \tag{8}$$

Note that (8) is consistent with (7) in the sense that they have the same solution.

1.2.2 Numerical experiments.

Algebraic solver robustness.

Kelvin–Helmholtz instability simulation.

1.3 Normal component equation. TBA...

2 Preliminaries

2.1 Bilinear forms and matrices. We set $n_{\mathbf{A}}$ to be the number of velocity d.o.f. and $n_{\mathbf{S}}$ to be the number of pressure d.o.f. Vector stiffness, divergence, pressure mass, normal stabilization, and full stabilization matrices resulting from Trace FEM discretization of the surface Stokes problem [4] are defined via

$$\begin{aligned}
 \langle \mathbf{A} \vec{\mathbf{u}}, \vec{\mathbf{v}} \rangle &\approx \int_{\Gamma} \left(2 E_{s,\Gamma}(\mathbf{u}) : E_{s,\Gamma}(\mathbf{v}) + \mathbf{u} \cdot \mathbf{v} + \tau (\mathbf{u} \cdot \mathbf{n}_{\Gamma}) (\mathbf{v} \cdot \mathbf{n}_{\Gamma}) \right) ds \\
 &\quad + \rho_u \int_{\Omega_h^{\Gamma}} \frac{\partial \mathbf{u}}{\partial \mathbf{n}_{\Gamma}} \cdot \frac{\partial \mathbf{v}}{\partial \mathbf{n}_{\Gamma}} dx, \quad \mathbf{A} \in \mathbb{R}^{n_{\mathbf{A}} \times n_{\mathbf{A}}}, \\
 \langle \mathbf{B} \vec{\mathbf{u}}, \vec{\mathbf{q}} \rangle &\approx \int_{\Gamma} \nabla_{\Gamma} q \cdot \mathbf{u} ds, \quad \mathbf{B} \in \mathbb{R}^{n_{\mathbf{S}} \times n_{\mathbf{A}}}, \\
 \langle \mathbf{M}_0 \vec{\mathbf{p}}, \vec{\mathbf{q}} \rangle &\approx \int_{\Gamma} p q ds, \quad \mathbf{M}_0 \in \mathbb{R}^{n_{\mathbf{S}} \times n_{\mathbf{S}}}, \\
 \langle \mathbf{C}_n \vec{\mathbf{p}}, \vec{\mathbf{q}} \rangle &\approx \rho_p \int_{\Omega_h^{\Gamma}} \frac{\partial p}{\partial \mathbf{n}_{\Gamma}} \frac{\partial q}{\partial \mathbf{n}_{\Gamma}} dx, \quad \mathbf{C}_n \in \mathbb{R}^{n_{\mathbf{S}} \times n_{\mathbf{S}}}, \\
 \langle \mathbf{C}_{\text{full}} \vec{\mathbf{p}}, \vec{\mathbf{q}} \rangle &\approx \rho_p \int_{\Omega_h^{\Gamma}} \nabla p \cdot \nabla q dx, \quad \mathbf{C}_{\text{full}} \in \mathbb{R}^{n_{\mathbf{S}} \times n_{\mathbf{S}}},
 \end{aligned} \tag{9}$$

respectively. We use notations as in [4], in particular, Ω_h^{Γ} is the domain consisting of tetrahedra cut by the surface $\Gamma := \{\mathbf{x} \in \mathbb{R}^3 : \phi(\mathbf{x}) = 0\}$. Here $\vec{\mathbf{u}}$ denotes a vector of d.o.f. corresponding to a FE interpolant \mathbf{u} (analogously for $\vec{\mathbf{p}}$ and p). See (13) and (14) for the computational details. Mesh-dependent parameters τ , ρ_u , and ρ_p are chosen to be proportional to some power of $h :=$ the typical mesh size for tetrahedra from Ω_h^{Γ} . Γ is chosen either as the unit sphere or torus, $\Gamma = \Gamma_{\text{sph}}$ or $\Gamma = \Gamma_{\text{tor}}$ (see Figure 1). The background domain is chosen as a cube $\Omega := (-5/3, 5/3)^3$.

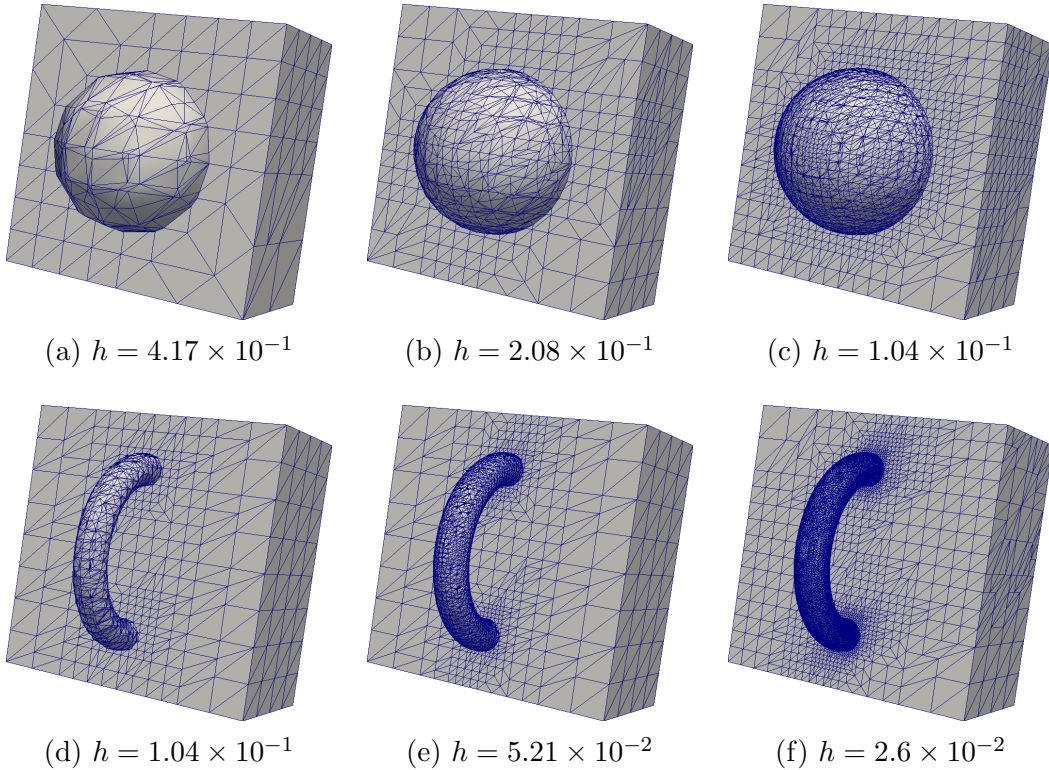


Figure 1: Cutaway of the bulk mesh and Γ_h for $\ell = 1, 2, 3$ for Γ_{sph} (top) and Γ_{tor} (bottom)

To build the initial triangulation, we divide Ω into 2^3 cubes and further tessellate each cube into 6 tetrahedra. Then the mesh is gradually refined towards the surface, and $\ell \in \mathbb{N}$ denotes the level of refinement, with the mesh size $h_\ell = \frac{5}{3} 2^{-\ell}$; see Figure 1 for the illustration of the bulk meshes and the induced mesh on the embedded surface for three consecutive refinement levels.

2.2 Quadratures for bilinear forms. We denote by $P_h^n \subset \bar{P}_h^n$ spaces of continuous and discontinuous nodal P_n interpolants defined on Ω_h^Γ , respectively. For a function f , $I_h^n(f) \in P_h^n$ is the corresponding interpolant; we will use the notation f_h^n to emphasize that $f_h^n \in P_h^n$ and f_h^n approximates f in some sense, but $I_h^n(f) \neq f_h^n$.

We set

$$\Gamma_h^n := \{\mathbf{x} \in \mathbb{R}^3 : (I_h^n(\phi))(\mathbf{x}) = 0\}, \quad (10)$$

$$\mathbf{n}_{\Gamma_h^n} = \frac{\nabla I_h^n(\phi)}{\|\nabla I_h^n(\phi)\|} \notin \bar{P}_h^m \text{ for any } m \text{ if } n > 1. \quad (11)$$

Note that Γ_h^n is a continuous piecewise P_n surface in Ω_h^Γ , and $\Gamma_h^n \neq I_h^n(\Gamma)$. The unit normal $\mathbf{n}_{\Gamma_h^n}$ is not a rational function; it is continuous in $T \in \Omega_h^\Gamma$ and discontinuous on faces. We also define

$$\Gamma_{h/m}^{2 \rightarrow 1} := \{\mathbf{x} \in \mathbb{R}^3 : (I_{h/m}^1(I_h^2(\phi)))(\mathbf{x}) = 0\}. \quad (12)$$

Note that $I_{h/2}^1(I_h^2(\phi)) = I_{h/2}^1(\phi)$ (since in order to build both $I_{h/2}^1$ and I_h^2 the same values of ϕ are used), and $I_{h/m}^1(I_h^2(\phi)) \neq I_{h/m}^1(\phi)$ for $m > 2$. Thus we have $\Gamma_{h/2}^{2 \rightarrow 1} = \Gamma_{h/2}^1$, and $\Gamma_{h/m}^{2 \rightarrow 1} \neq \Gamma_{h/m}^1$ for $m > 2$. We refer to Figures 2 and 3.

We implemented two options for the matrix assembly (9). The first one is

$$\begin{aligned} \langle \mathbf{A} \vec{\mathbf{u}}, \vec{\mathbf{v}} \rangle &= \int_{\Gamma_{h/m}^{2 \rightarrow 1}}^5 (2 E_{s, \Gamma_h^2}(\mathbf{u}) : E_{s, \Gamma_h^2}(\mathbf{v}) + \mathbf{u} \cdot \mathbf{v} + \tau (\mathbf{u} \cdot \mathbf{n}_{\Gamma_h^2})(\mathbf{v} \cdot \mathbf{n}_{\Gamma_h^2})) \, ds \\ &\quad + \rho_u \int_{\Omega_h^\Gamma} \frac{\partial \mathbf{u}}{\partial \mathbf{n}_{\Gamma_h^2}} \cdot \frac{\partial \mathbf{v}}{\partial \mathbf{n}_{\Gamma_h^2}} \, d\mathbf{x}, \quad \mathbf{A} \in \mathbb{R}^{n_A \times n_A}, \\ \langle \mathbf{B} \vec{\mathbf{u}}, \vec{\mathbf{q}} \rangle &= \int_{\Gamma_{h/m}^{2 \rightarrow 1}}^5 \nabla_{\Gamma_h^2} q \cdot \mathbf{u} \, ds, \quad \mathbf{B} \in \mathbb{R}^{n_S \times n_A}, \\ \langle \mathbf{M}_0 \vec{\mathbf{p}}, \vec{\mathbf{q}} \rangle &= \int_{\Gamma_{h/m}^{2 \rightarrow 1}}^5 p q \, ds, \quad \mathbf{M}_0 \in \mathbb{R}^{n_S \times n_S}, \\ \langle \mathbf{C}_n \vec{\mathbf{p}}, \vec{\mathbf{q}} \rangle &= \rho_p \int_{\Omega_h^\Gamma} \frac{\partial p}{\partial \mathbf{n}_{\Gamma_h^2}} \frac{\partial q}{\partial \mathbf{n}_{\Gamma_h^2}} \, d\mathbf{x}, \quad \mathbf{C}_n \in \mathbb{R}^{n_S \times n_S}, \\ \langle \mathbf{C}_{\text{full}} \vec{\mathbf{p}}, \vec{\mathbf{q}} \rangle &= \rho_p \int_{\Omega_h^\Gamma} \nabla p \cdot \nabla q \, d\mathbf{x}, \quad \mathbf{C}_{\text{full}} \in \mathbb{R}^{n_S \times n_S}. \end{aligned} \quad (13)$$

- $\int_{\Gamma_{h/m}^{2 \rightarrow 1}}^5 \cdot \, ds$ denotes a composite quadrature rule that is exact for $\bar{P}_h^5(\Gamma_{h/m}^{2 \rightarrow 1})$, i.e. this quadrature is exact for piecewise polynomials up to degree 5 on each triangular patch $\gamma \in \Gamma_{h/m}^{2 \rightarrow 1}$,
- $\int_{\Omega_h^\Gamma}^5 \cdot \, d\mathbf{x}$ denotes a composite quadrature rule that is exact for $\bar{P}_h^5(\Omega_h^\Gamma)$, i.e. this quadrature is exact for piecewise polynomials up to degree 5 on each tetrahedron $T \in \Omega_h^\Gamma$,
- E_{s, Γ_h^2} and $\nabla_{\Gamma_h^2}$ are defined as their continuous analogues with \mathbf{n}_Γ in \mathbf{P}_Γ replaced with $\mathbf{n}_{\Gamma_h^2}$.

The second option is

$$\begin{aligned}
\langle \mathbf{A} \vec{\mathbf{u}}, \vec{\mathbf{v}} \rangle &= \int_{\Gamma_{h/m}^{2 \rightarrow 1}}^5 \left(2 E_{s, \Gamma_{h/m}^{2 \rightarrow 1}}(\mathbf{u}) : E_{s, \Gamma_{h/m}^{2 \rightarrow 1}}(\mathbf{v}) + \mathbf{u} \cdot \mathbf{v} + \tau (\mathbf{u} \cdot \mathbf{n}_{\Gamma_h^2}) (\mathbf{v} \cdot \mathbf{n}_{\Gamma_h^2}) \right) ds \\
&\quad + \rho_u \int_{\Omega_h^\Gamma} \frac{\partial \mathbf{u}}{\partial \mathbf{n}_{\Gamma_h^2}} \cdot \frac{\partial \mathbf{v}}{\partial \mathbf{n}_{\Gamma_h^2}} d\mathbf{x}, \quad \mathbf{A} \in \mathbb{R}^{n_A \times n_A}, \\
\langle \mathbf{B} \vec{\mathbf{u}}, \vec{\mathbf{q}} \rangle &= \int_{\Gamma_{h/m}^{2 \rightarrow 1}}^5 \nabla_{\Gamma_{h/m}^{2 \rightarrow 1}} q \cdot \mathbf{u} ds, \quad \mathbf{B} \in \mathbb{R}^{n_S \times n_A}, \\
\langle \mathbf{M}_0 \vec{\mathbf{p}}, \vec{\mathbf{q}} \rangle &= \int_{\Gamma_{h/m}^{2 \rightarrow 1}}^5 p q ds, \quad \mathbf{M}_0 \in \mathbb{R}^{n_S \times n_S}, \\
\langle \mathbf{C}_n \vec{\mathbf{p}}, \vec{\mathbf{q}} \rangle &= \rho_p \int_{\Omega_h^\Gamma} \frac{\partial p}{\partial \mathbf{n}_{\Gamma_h^2}} \frac{\partial q}{\partial \mathbf{n}_{\Gamma_h^2}} d\mathbf{x}, \quad \mathbf{C}_n \in \mathbb{R}^{n_S \times n_S}, \\
\langle \mathbf{C}_{\text{full}} \vec{\mathbf{p}}, \vec{\mathbf{q}} \rangle &= \rho_p \int_{\Omega_h^\Gamma} \nabla p \cdot \nabla q d\mathbf{x}, \quad \mathbf{C}_{\text{full}} \in \mathbb{R}^{n_S \times n_S}.
\end{aligned} \tag{14}$$

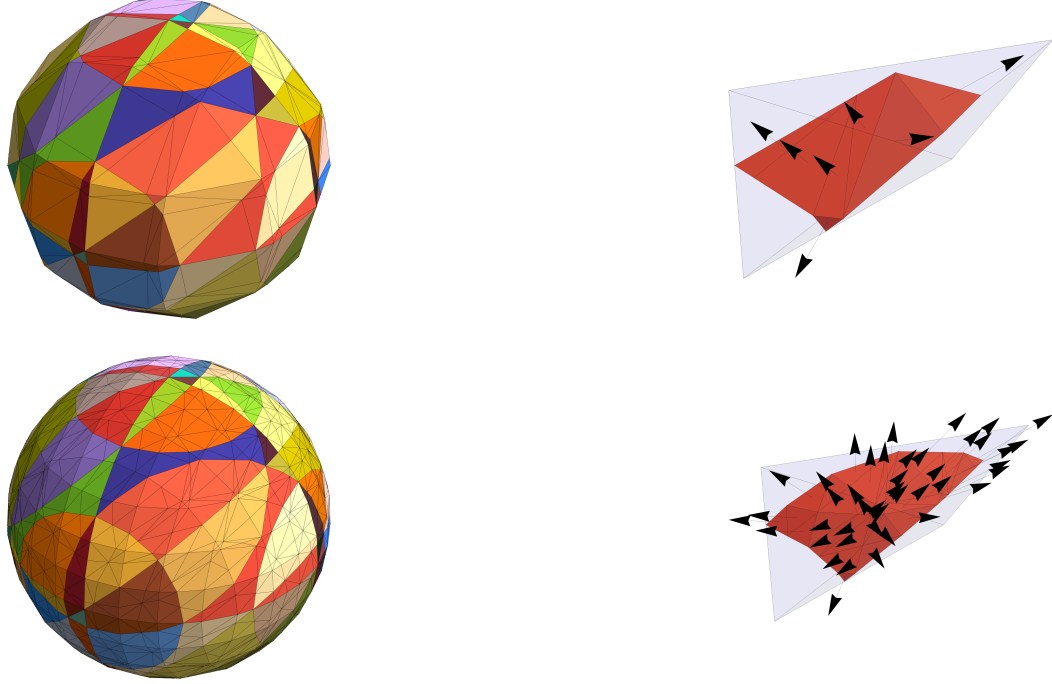


Figure 2: $\Gamma = \Gamma_{\text{sph}}$, $\phi(\mathbf{x}) = \|\mathbf{x}\|^2 - 1$, $h = 8.33 \times 10^{-1}$. Top-left: triangular patches $\gamma \in \Gamma_{h/2}^{2 \rightarrow 1} = \Gamma_{h/2}^1$ (different color corresponds to a different tetrahedron $T \in \Omega_h^\Gamma$). Top-right: a patch γ and its normals. Bottom-left and bottom-right: same for $\Gamma_{h/4}^{2 \rightarrow 1} = \Gamma_{h/4}^1$. Note that since $\phi \in P^2$, we have that $\Gamma_{h/m}^{2 \rightarrow 1} = \Gamma_{h/m}^1 \rightarrow \Gamma$ as $m \rightarrow \infty$ even for fixed h

For both formulations (13) and (14) the loading vectors for moments and continuity equations are approx-

imated as

$$\begin{aligned}\mathbf{f}_i &= \int_{\Gamma_{h/m}^{2 \rightarrow 1}}^5 \mathbf{f} \cdot \boldsymbol{\phi}_i \, ds, \quad i = 1, 2, \dots, n_{\mathbf{A}}, \\ \mathbf{g}_i &= - \int_{\Gamma_{h/m}^{2 \rightarrow 1}}^5 g \phi_i \, ds, \quad i = 1, 2, \dots, n_{\mathbf{S}},\end{aligned}\tag{15}$$

respectively. Here $\boldsymbol{\phi}_i$ and ϕ_i are vector and scalar Lagrange basis functions defined on Ω_h^Γ .



Figure 3: $\Gamma = \Gamma_{\text{sph}}$, $\phi(\mathbf{x}) = \|\mathbf{x}\|^{1/2} - 1$, $h = 8.33 \times 10^{-1}$. Left: triangular patches $\gamma \in \Gamma_{h/2}^1$ (different color corresponds to a different tetrahedron $T \in \Omega_h^\Gamma$). Right: same for $\Gamma_{h/4}^{2 \rightarrow 1} \neq \Gamma_{h/4}^1$. **Note that since $\phi \notin \bar{P}_h^2$, we have that $\Gamma_{h/m}^{2 \rightarrow 1} \neq \Gamma_{h/m}^1$ for $m > 2$, and $\Gamma_{h/m}^{2 \rightarrow 1} \rightarrow \Gamma_h^2 \neq \Gamma$ as $m \rightarrow \infty$ for fixed h**

As in [2], we refer to (9) as **inconsistent formulation**. We also consider the same formulation as in (9) but with the first term \mathbf{A}_s in the definition of \mathbf{A} changed as

$$\langle \mathbf{A}_s \vec{\mathbf{u}}, \vec{\mathbf{v}} \rangle \approx \int_{\Gamma} 2(E_{s,\Gamma}(\mathbf{u}) - (\mathbf{u} \cdot \mathbf{n}_{\Gamma}) \mathbf{H}_{\Gamma}) : (E_{s,\Gamma}(\mathbf{v}) - (\mathbf{v} \cdot \mathbf{n}_{\Gamma}) \mathbf{H}_{\Gamma}) \, ds, \tag{16}$$

where the shape operator is defined as $\mathbf{H}_{\Gamma} := \nabla_{\Gamma} \mathbf{n}_{\Gamma} := \mathbf{P}_{\Gamma} \nabla \mathbf{n}_{\Gamma}^e \mathbf{P}_{\Gamma}$, $\mathbf{H}_{\Gamma} : \mathcal{O}(\Gamma) \rightarrow \mathbb{R}^3$. We refer to (16) as **consistent formulation**.

Similarly to (13) and (14), we consider two discretizations of (16):

$$\langle \mathbf{A}_s \vec{\mathbf{u}}, \vec{\mathbf{v}} \rangle = \int_{\Gamma_{h/m}^{2 \rightarrow 1}}^5 2(E_{s,\Gamma_h^2}(\mathbf{u}) - (\mathbf{u} \cdot \mathbf{n}_{\Gamma_h^2}) \mathbf{H}_{\Gamma_h^2}) : (E_{s,\Gamma_h^2}(\mathbf{v}) - (\mathbf{v} \cdot \mathbf{n}_{\Gamma_h^2}) \mathbf{H}_{\Gamma_h^2}) \, ds \tag{17}$$

and

$$\langle \mathbf{A}_s \vec{\mathbf{u}}, \vec{\mathbf{v}} \rangle = \int_{\Gamma_{h/m}^{2 \rightarrow 1}}^5 2(E_{s,\Gamma_{h/m}^{2 \rightarrow 1}}(\mathbf{u}) - (\mathbf{u} \cdot \mathbf{n}_{\Gamma_{h/m}^{2 \rightarrow 1}}) \mathbf{H}_{\Gamma_{h/m}^{2 \rightarrow 1}}) : (E_{s,\Gamma_{h/m}^{2 \rightarrow 1}}(\mathbf{v}) - (\mathbf{v} \cdot \mathbf{n}_{\Gamma_{h/m}^{2 \rightarrow 1}}) \mathbf{H}_{\Gamma_{h/m}^{2 \rightarrow 1}}) \, ds. \tag{18}$$

Note that $\mathbf{n}_{\Gamma} = \nabla \phi / \|\nabla \phi\|$ is defined in $\mathcal{O}(\Gamma)$, so $\nabla \mathbf{n}_{\Gamma}$ makes sense and

$$\nabla \mathbf{n}_{\Gamma} = \left(\mathbf{I} - \frac{\nabla \phi \nabla \phi^T}{\|\nabla \phi\|^2} \right) \frac{\nabla^2 \phi}{\|\nabla \phi\|} = \mathbf{P}_{\Gamma} \frac{\nabla^2 \phi}{\|\nabla \phi\|}.$$

If $\mathbf{n}_{\Gamma} = \mathbf{n}_{\Gamma}^e$, one gets

$$\mathbf{H}_{\Gamma} = \mathbf{P}_{\Gamma} \frac{\nabla^2 \phi}{\|\nabla \phi\|} \mathbf{P}_{\Gamma}. \tag{19}$$

Thus we define $\mathbf{H}_{\Gamma_h^2}$ to be as in (19) but with ϕ replaced with $I_h^2(\phi)$, i.e.

$$\mathbf{H}_{\Gamma_h^2} := \mathbf{P}_{\Gamma_h^2} \frac{\nabla^2 I_h^2(\phi)}{\|\nabla I_h^2(\phi)\|} \mathbf{P}_{\Gamma_h^2}. \quad (20)$$

Indeed, computation of $\mathbf{H}_{\Gamma_h^2}$ requires Hessians of shape functions.

Depending on the choice of ϕ , we may or may not have $\mathbf{n}_\Gamma = \mathbf{n}_\Gamma^e$. Note that the choice $\phi = d$ is sufficient for this, but not necessary. Consider this choices of ϕ for Γ_{sph} :

1. $\phi_1(\mathbf{x}) = \|\mathbf{x}\| - 1 = d(\mathbf{x})$, $\nabla\phi_1/\|\nabla\phi_1\| = \mathbf{n}_\Gamma^e$,
2. $\phi_2(\mathbf{x}) = \|\mathbf{x}\|^2 - 1 \in P^2$, $\nabla\phi_2/\|\nabla\phi_2\| = \nabla\phi_1/\|\nabla\phi_1\| = \mathbf{n}_\Gamma^e$,
3. $\phi_3(\mathbf{x}) = e^{\phi_2(\mathbf{x})} x^2 + y^2 + z^2 - 1$, $\nabla\phi_3/\|\nabla\phi_3\| \neq \mathbf{n}_\Gamma^e$, i.e. $\nabla\phi_3/\|\nabla\phi_3\| = \mathbf{n}_\Gamma$ only on Γ_{sph} .

As for the case 2: note that if ϕ is piecewise quadratic in Ω_h^Γ and defines a normal that is equal to its extension, then $\mathbf{H}_{\Gamma_h^2} = \mathbf{H}_\Gamma$, i.e. the approximation is **exact**.

For the approach (14), there is also an option to approximate \mathbf{H} as $\mathbf{P}_{\Gamma_{h/m}^{2 \rightarrow 1}} \frac{\nabla^2 I_h^2(\phi)}{\|\nabla I_h^2(\phi)\|} \mathbf{P}_{\Gamma_{h/m}^{2 \rightarrow 1}}$ since we build $\mathbf{P}_{\Gamma_{h/m}^{2 \rightarrow 1}}$ anyway. We chose to use (20) for both (13) and (14).

2.3 Error computation. Note that $\mathbb{H}^1(\Gamma)$ -error (for e.g. $\mathbf{P}_2 - P_1$ FE) can be cheaply approximated as $\langle \mathbf{w}, \mathbf{A}_s \mathbf{w} \rangle^{1/2}$, $\mathbf{w} :=$ vector of d.o.f. corresponding to \mathbf{P}_h^2 interpolant $I_h^2(\mathbf{u}^e) - \mathbf{u}_h$, $\mathbf{A}_s :=$ matrix corresponding to the first term of \mathbf{A} in (14). Thus the errors are approximated as

$$\begin{aligned} \|\mathbf{u} - \mathbf{u}_h\|_{\mathbb{H}^1(\Gamma)} &= \|I_h^k(\mathbf{u}^e) - \mathbf{u}_h\|_{\mathbb{H}^1(\Gamma_{h/m}^{2 \rightarrow 1})} + O(h^k), \\ \|\mathbf{u} - \mathbf{u}_h\|_{\mathbb{L}^2(\Gamma)} &= \|I_h^k(\mathbf{u}^e) - \mathbf{u}_h\|_{\mathbb{L}^2(\Gamma_{h/m}^{2 \rightarrow 1})} + O(h^{k+1}), \\ \|p - p_h\|_{\mathbb{L}^2(\Gamma)} &= \|I_h^1(p^e) - p_h\|_{\mathbb{L}^2(\Gamma_{h/m}^{2 \rightarrow 1})} + O(h^2) \end{aligned} \quad (21)$$

for $m > 1$. Here $k = 1$ for $\mathbf{P}_1 - P_1$ FEM and $k = 2$ for $\mathbf{P}_2 - P_1$. For consistent penalty approach matrix \mathbf{A}_s is computed as in (17) or (18).

3 Convergence results

3.1 Manufactured solution. We solve model problem from [4, p. 20], $\Gamma = \Gamma_{\text{sph}}^1$. We set

$$\tilde{\mathbf{u}}(x, y, z) := (-z^2, y, x)^T, \quad \tilde{p}(x, y, z) := xy^2 + z, \quad \phi(\mathbf{x}) := \|\mathbf{x}\|^2 - 1. \quad (22)$$

The exact solution on the unit sphere is chosen as

$$\mathbf{u} := \mathbf{P}_\Gamma \tilde{\mathbf{u}}^e, \quad p := \tilde{p}^e. \quad (23)$$

Thus we have $\int_\Gamma p \, d\mathbf{x} = 0$, $p \equiv p^e$, $\mathbf{u} \equiv \mathbf{u}^e$ in $\mathcal{O}(\Gamma)$, and \mathbf{u} is a tangential field. Note that for our choice of ϕ in (22) we have

$$\mathbf{n}_{\Gamma_h^2} = \mathbf{n}_\Gamma^e \text{ in } \mathcal{O}(\Gamma), \quad \Gamma_{h/m}^{2 \rightarrow 1} = \Gamma_{h/m}^1, \quad \mathbf{n}_{\Gamma_{h/m}^{2 \rightarrow 1}} = \mathbf{n}_{\Gamma_{h/m}^1} \text{ on } \Gamma, \quad (24)$$

and

$$\mathbf{n}_{\Gamma_{h/m}^1} \rightarrow \mathbf{n}_\Gamma, \quad \Gamma_{h/m}^1 \rightarrow \Gamma \quad (25)$$

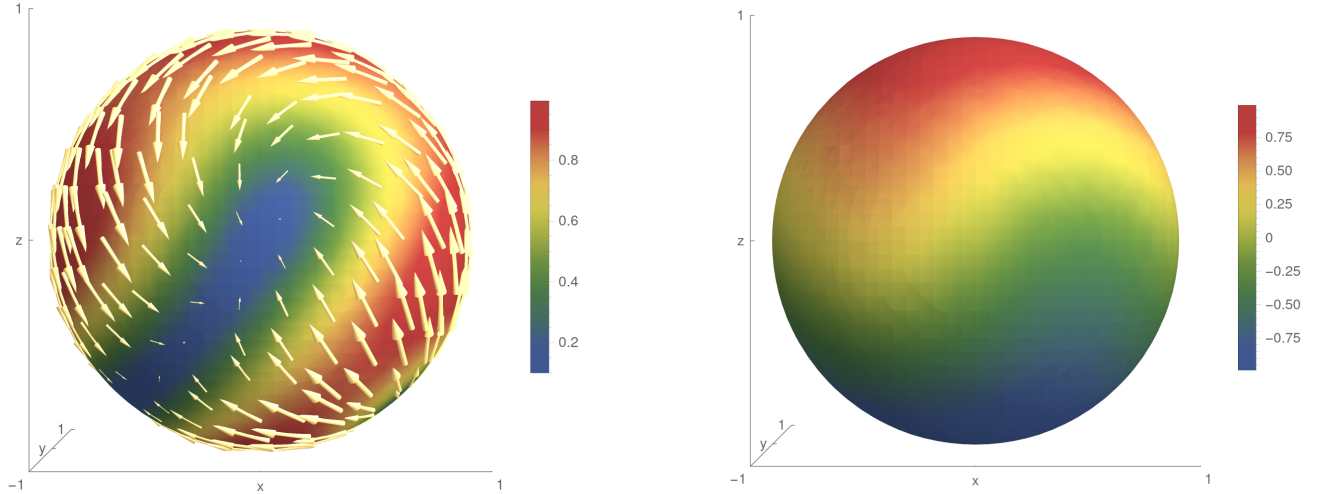


Figure 4: Exact velocity solution (Left) and pressure solution (Right) as in (23)

as one increases m **even for fixed h** .

We have

$$\mathbf{n}_{\Gamma_{\text{sph}}}(\mathbf{x}) = \|\mathbf{x}\|^{-1} \mathbf{x} = \mathbf{n}_{\Gamma_{\text{sph}}}^e(\mathbf{x}), \quad (26)$$

$$\mathbf{P}_{\Gamma_{\text{sph}}}(\mathbf{x}) = \|\mathbf{x}\|^{-2} \begin{pmatrix} y^2 + z^2 & -xy & -xz \\ -xy & x^2 + z^2 & -yz \\ -xz & -yz & x^2 + y^2 \end{pmatrix} = \mathbf{P}_{\Gamma_{\text{sph}}}^e(\mathbf{x}), \quad (27)$$

$$\mathbf{H}_{\Gamma_{\text{sph}}}(\mathbf{x}) = \|\mathbf{x}\|^{-3} \begin{pmatrix} y^2 + z^2 & -xy & -xz \\ -xy & x^2 + z^2 & -yz \\ -xz & -yz & x^2 + y^2 \end{pmatrix} \neq \mathbf{H}_{\Gamma_{\text{sph}}}^e(\mathbf{x}) = \mathbf{P}_{\Gamma_{\text{sph}}}(\mathbf{x}). \quad (28)$$

We consider two choices for virtual refinement: $m \propto h^{-1/2}$ and $m \propto h^{-1}$. The first choice assures h^3 -accurate approximation of Γ and $h^{3/2}$ accurate approximation of the normal vector, whereas the second choice assures h^4 - and h^2 -approximations. We refer to Figure 5.

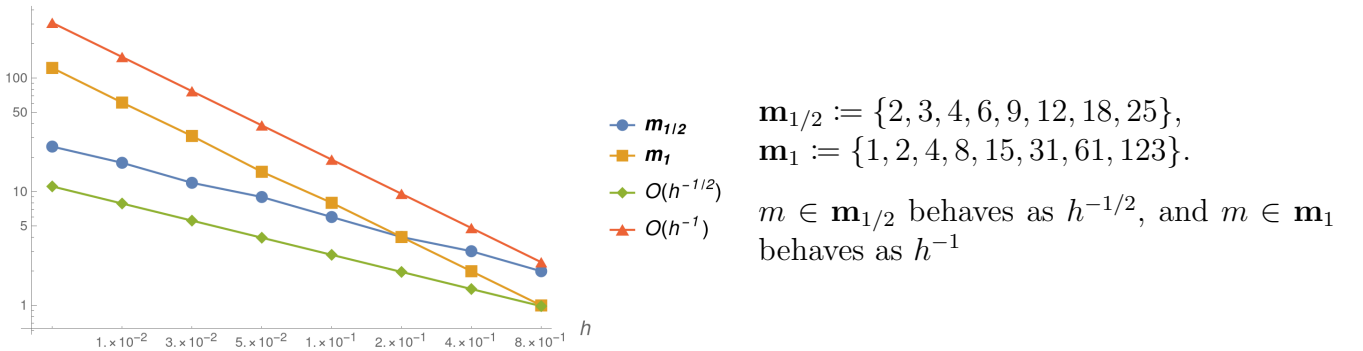


Figure 5: Virtual refinement parameter m for $\Gamma_{h/m}^{2 \rightarrow 1}$

¹In [4] they use $\mathbf{u} := \mathbf{P} \tilde{\mathbf{u}}$, i.e. $\mathbf{u} \neq \mathbf{u}^e$. I prefer $\mathbf{u} \equiv \mathbf{u}^e$ as in [2].

Table 1: Errors for normals and shape operator, $\Gamma = \Gamma_{\text{sph}}$. Please see (24) and (25)

$m \in \mathbf{m}_{1/2}$ as in Figure 5					
h	$\ \mathbf{n}_\Gamma^e - \mathbf{n}_{\Gamma_h^2}\ _{\mathbb{L}^2(\Gamma_{h/m}^1)}$	$\ \mathbf{n}_\Gamma^e - \mathbf{n}_{\Gamma_{h/m}^1}\ _{\mathbb{L}^2(\Gamma_{h/m}^1)}$	Order	$\ \mathbf{H}_\Gamma^e - \mathbf{H}_{\Gamma_h^2}\ _{\mathbb{L}^2(\Gamma_{h/m}^1)}$	Order
8.3×10^{-1}	8.1×10^{-16}	6.4×10^{-1}		2.3×10^{-1}	
4.2×10^{-1}	1.1×10^{-15}	$2. \times 10^{-1}$	1.7	2.5×10^{-2}	3.2
2.1×10^{-1}	2.3×10^{-15}	7.6×10^{-2}	1.4	3.5×10^{-3}	2.8
$1. \times 10^{-1}$	5.2×10^{-15}	2.5×10^{-2}	1.6	3.9×10^{-4}	3.2
5.2×10^{-2}	9.3×10^{-15}	8.4×10^{-3}	1.6	4.3×10^{-5}	3.2
2.6×10^{-2}	1.9×10^{-14}	3.1×10^{-3}	1.4	6.1×10^{-6}	2.8
1.3×10^{-2}	3.6×10^{-14}	$1. \times 10^{-3}$	1.6	6.8×10^{-7}	3.2

3.2 $P_2 - P_1$ Trace FEM. Next we compare inconsistent and consistent Trace FEM penalty formulations.

3.2.1 Inconsistent penalty formulation. We use the normal stabilization matrix \mathbf{C}_n . We stick to the approach (13), so with (24) we have

$$\begin{aligned}
 \langle \mathbf{A} \vec{\mathbf{u}}, \vec{\mathbf{v}} \rangle &= \int_{\Gamma_{h/2}^1} \left(2 E_{s,\Gamma}(\mathbf{u}) : E_{s,\Gamma}(\mathbf{v}) + \mathbf{u} \cdot \mathbf{v} + \tau (\mathbf{u} \cdot \mathbf{n}_\Gamma) (\mathbf{v} \cdot \mathbf{n}_\Gamma) \right) ds \\
 &\quad + \rho_u \int_{\Omega_h^\Gamma} \frac{\partial \mathbf{u}}{\partial \mathbf{n}_\Gamma} \cdot \frac{\partial \mathbf{v}}{\partial \mathbf{n}_\Gamma} d\mathbf{x}, \quad \mathbf{A} \in \mathbb{R}^{n_A \times n_A}, \\
 \langle \mathbf{B} \vec{\mathbf{u}}, \vec{\mathbf{q}} \rangle &= \int_{\Gamma_{h/2}^1} \nabla_\Gamma q \cdot \mathbf{u} ds, \quad \mathbf{B} \in \mathbb{R}^{n_S \times n_A}, \\
 \langle \mathbf{M}_0 \vec{\mathbf{p}}, \vec{\mathbf{q}} \rangle &= \int_{\Gamma_{h/2}^1} p q ds, \quad \mathbf{M}_0 \in \mathbb{R}^{n_S \times n_S}, \\
 \langle \mathbf{C}_n \vec{\mathbf{p}}, \vec{\mathbf{q}} \rangle &= \rho_p \int_{\Omega_h^\Gamma} \frac{\partial p}{\partial \mathbf{n}_\Gamma} \frac{\partial q}{\partial \mathbf{n}_\Gamma} d\mathbf{x}, \quad \mathbf{C}_n \in \mathbb{R}^{n_S \times n_S}.
 \end{aligned} \tag{29}$$

Table 2: Convergence results. $\tau = h^{-2}$, $\rho_u = h$, $\rho_p = h$. Matrices are assembled as in (29)

$m \in \mathbf{m}_{1/2}$ as in Figure 5						
h	$\ \mathbf{u} - \mathbf{u}_h\ _{\mathbb{H}^1}$	Order	$\ \mathbf{u} - \mathbf{u}_h\ _{\mathbb{L}^2}$	Order	$\ p - p_h\ _{\mathbb{L}^2}$	Order
8.3×10^{-1}	3.		1.8		2.1	
4.2×10^{-1}	1.8	7.4×10^{-1}	9.1×10^{-1}	9.7×10^{-1}	1.7	2.7×10^{-1}
2.1×10^{-1}	$7. \times 10^{-1}$	1.4	3.4×10^{-1}	1.4	6.9×10^{-1}	1.3
$1. \times 10^{-1}$	$2. \times 10^{-1}$	1.8	9.9×10^{-2}	1.8	$2. \times 10^{-1}$	1.8
5.2×10^{-2}	5.2×10^{-2}	1.9	2.6×10^{-2}	1.9	5.2×10^{-2}	1.9
2.6×10^{-2}	1.3×10^{-2}	2.	6.5×10^{-3}	2.	1.3×10^{-2}	2.
1.3×10^{-2}	3.3×10^{-3}	2.	1.6×10^{-3}	2.	3.3×10^{-3}	2.

h	$\ \mathbf{u}_h \cdot \mathbf{n}\ _{\mathbb{L}^2}$	Order	Outer iterations	Residual norm
8.33×10^{-1}	1.8		24	6.2×10^{-9}
4.17×10^{-1}	9.2×10^{-1}	9.4×10^{-1}	31	5.4×10^{-9}
2.08×10^{-1}	3.5×10^{-1}	1.4	30	9.8×10^{-9}
1.04×10^{-1}	9.9×10^{-2}	1.8	27	7.8×10^{-9}
5.21×10^{-2}	2.6×10^{-2}	1.9	26	8.3×10^{-9}
2.6×10^{-2}	6.5×10^{-3}	2.	26	9.6×10^{-9}
1.3×10^{-2}	1.6×10^{-3}	2.	35	$7. \times 10^{-9}$

For statistics: using 64 CPUs, computation of the meshlevel 3 ($h = 2.08 \times 10^{-1}$) takes ~ 1 minute, meshlevel 4 takes ~ 7 minutes, meshlevel 5 takes ~ 50 minutes, meshlevel 6 takes 4.8 hours, and meshlevel 7 takes ~ 21.3 hours.

3.2.2 Consistent penalty formulation. We consider the same formulation as in (29), but with the first term \mathbf{A}_s in the definition of \mathbf{A} changed according to (17). Thus with (24) we have

$$\langle \mathbf{A}_s \vec{\mathbf{u}}, \vec{\mathbf{v}} \rangle = \int_{\Gamma_{h/m}^1}^5 2(E_{s,\Gamma}(\mathbf{u}) - (\mathbf{u} \cdot \mathbf{n}_\Gamma) \mathbf{H}_\Gamma) : (E_{s,\Gamma}(\mathbf{v}) - (\mathbf{v} \cdot \mathbf{n}_\Gamma) \mathbf{H}_\Gamma) \, ds. \quad (30)$$

Table 3: Convergence results. $\tau = h^{-2}$, $\rho_u = h^{-1}$, $\rho_p = h$, $\mathbf{C}_\star = \mathbf{C}_{\text{full}}$. Matrices are assembled as in (29)–(30)

$m \in \mathbf{m}_{1/2}$ as in Figure 5						
h	$\ \mathbf{u} - \mathbf{u}_h\ _{\mathbb{H}^1}$	Order	$\ \mathbf{u} - \mathbf{u}_h\ _{\mathbb{L}^2}$	Order	$\ p - p_h\ _{\mathbb{L}^2}$	Order
8.3×10^{-1}	1.6		7.8×10^{-1}		1.3	
4.2×10^{-1}	6.9×10^{-1}	1.2	3.9×10^{-1}	1.	8.1×10^{-1}	6.3×10^{-1}
2.1×10^{-1}	2.4×10^{-1}	1.5	1.3×10^{-1}	1.6	3.1×10^{-1}	1.4
$1. \times 10^{-1}$	8.1×10^{-2}	1.6	3.6×10^{-2}	1.8	1.1×10^{-1}	1.5
5.2×10^{-2}	2.4×10^{-2}	1.8	9.5×10^{-3}	1.9	3.2×10^{-2}	1.7
2.6×10^{-2}	6.5×10^{-3}	1.9	2.4×10^{-3}	2.	8.8×10^{-3}	1.9
1.3×10^{-2}	1.8×10^{-3}	1.8	6.1×10^{-4}	2.	2.5×10^{-3}	1.8

h	$\ \mathbf{u}_h \cdot \mathbf{n}\ _{\mathbb{L}^2}$	Order	Outer iterations	Residual norm
8.33×10^{-1}	3.5×10^{-1}		15	1.3×10^{-9}
4.17×10^{-1}	5.4×10^{-2}	2.7	21	3.5×10^{-9}
2.08×10^{-1}	4.9×10^{-3}	3.4	27	5.5×10^{-9}
1.04×10^{-1}	$5. \times 10^{-4}$	3.3	29	5.8×10^{-9}
5.21×10^{-2}	4.9×10^{-5}	3.4	29	5.1×10^{-9}
2.6×10^{-2}	$5. \times 10^{-6}$	3.3	28	8.4×10^{-9}
1.3×10^{-2}	5.9×10^{-7}	3.1	34	9.1×10^{-9}

Table 4: Convergence results. $\tau = h^{-2}$, $\rho_u = h^{-1}$, $\rho_p = h$, $\mathbf{C}_\star = \mathbf{C}_n$. Matrices are assembled as in (29)–(30)

$m \in \mathbf{m}_{1/2}$ as in Figure 5						
h	$\ \mathbf{u} - \mathbf{u}_h\ _{\mathbb{H}^1}$	Order	$\ \mathbf{u} - \mathbf{u}_h\ _{\mathbb{L}^2}$	Order	$\ p - p_h\ _{\mathbb{L}^2}$	Order
8.3×10^{-1}	1.2		4.8×10^{-1}		4.2×10^{-1}	
4.2×10^{-1}	3.7×10^{-1}	1.8	6.1×10^{-2}	3.	1.1×10^{-1}	2.
2.1×10^{-1}	9.2×10^{-2}	2.	5.8×10^{-3}	3.4	2.5×10^{-2}	2.1
$1. \times 10^{-1}$	2.2×10^{-2}	2.1	5.6×10^{-4}	3.4	6.3×10^{-3}	2.
5.2×10^{-2}	5.4×10^{-3}	2.	5.2×10^{-5}	3.4	1.7×10^{-3}	1.8
2.6×10^{-2}	1.4×10^{-3}	2.	5.4×10^{-6}	3.3	5.3×10^{-4}	1.7
1.3×10^{-2}	3.5×10^{-4}	2.	6.9×10^{-7}	3.	1.8×10^{-4}	1.6

h	$\ \mathbf{u}_h \cdot \mathbf{n}\ _{\mathbb{L}^2}$	Order	Outer iterations	Residual norm
8.33×10^{-1}	3.4×10^{-1}		26	7.3×10^{-9}
4.17×10^{-1}	5.3×10^{-2}	2.7	33	4.8×10^{-9}
2.08×10^{-1}	4.9×10^{-3}	3.4	31	$6. \times 10^{-9}$
1.04×10^{-1}	$5. \times 10^{-4}$	3.3	27	8.3×10^{-9}
5.21×10^{-2}	4.9×10^{-5}	3.4	26	8.6×10^{-9}
2.6×10^{-2}	$5. \times 10^{-6}$	3.3	26	7.5×10^{-9}
1.3×10^{-2}	5.9×10^{-7}	3.1	34	$8. \times 10^{-9}$

$m \in \mathbf{m}_1$ as in Figure 5						
h	$\ \mathbf{u} - \mathbf{u}_h\ _{\mathbb{H}^1}$	Order	$\ \mathbf{u} - \mathbf{u}_h\ _{\mathbb{L}^2}$	Order	$\ p - p_h\ _{\mathbb{L}^2}$	Order
8.3×10^{-1}	2.2		6.4×10^{-1}		7.4×10^{-1}	
4.2×10^{-1}	3.8×10^{-1}	2.5	6.1×10^{-2}	3.4	1.2×10^{-1}	2.6
2.1×10^{-1}	9.2×10^{-2}	2.1	5.8×10^{-3}	3.4	2.5×10^{-2}	2.2
$1. \times 10^{-1}$	2.2×10^{-2}	2.1	5.6×10^{-4}	3.4	6.1×10^{-3}	2.1
5.2×10^{-2}	5.3×10^{-3}	2.	5.2×10^{-5}	3.4	1.6×10^{-3}	1.9
2.6×10^{-2}	1.3×10^{-3}	2.	5.2×10^{-6}	3.3	4.1×10^{-4}	2.
1.3×10^{-2}	3.4×10^{-4}	2.	$6. \times 10^{-7}$	3.1	$1. \times 10^{-4}$	2.

h	$\ \mathbf{u}_h \cdot \mathbf{n}\ _{\mathbb{L}^2}$	Order	Outer iterations	Residual norm
8.33×10^{-1}	4.5×10^{-1}		26	2.6×10^{-9}
4.17×10^{-1}	5.3×10^{-2}	3.1	33	5.1×10^{-9}
2.08×10^{-1}	4.9×10^{-3}	3.4	31	$6. \times 10^{-9}$
1.04×10^{-1}	$5. \times 10^{-4}$	3.3	27	7.3×10^{-9}
5.21×10^{-2}	4.9×10^{-5}	3.4	25	6.4×10^{-9}
2.6×10^{-2}	$5. \times 10^{-6}$	3.3	26	4.3×10^{-9}
1.3×10^{-2}	5.8×10^{-7}	3.1	34	7.8×10^{-9}

For statistics: using 80 CPUs, computation of the meshlevel 7 ($h = 1.3 \times 10^{-2}$) takes ~ 27 hours with $m = 18$ (computation also involves errors for normals and the shape operator).

Table 6: Convergence results. $\tau = h^{-2}$, $\rho_u = h^{-1}$, $\rho_p = 1$, $\mathbf{C}_\star = \mathbf{C}_n$. Matrices are assembled as in (29)–(30)

$m \in \mathbf{m}_{1/2}$ as in Figure 5						
h	$\ \mathbf{u} - \mathbf{u}_h\ _{\mathbb{H}^1}$	Order	$\ \mathbf{u} - \mathbf{u}_h\ _{\mathbb{L}^2}$	Order	$\ p - p_h\ _{\mathbb{L}^2}$	Order
8.3×10^{-1}	1.3		$5. \times 10^{-1}$		4.9×10^{-1}	
4.2×10^{-1}	3.8×10^{-1}	1.7	6.7×10^{-2}	2.9	1.5×10^{-1}	1.7
2.1×10^{-1}	$1. \times 10^{-1}$	1.9	8.6×10^{-3}	3.	$5. \times 10^{-2}$	1.5
$1. \times 10^{-1}$	2.4×10^{-2}	2.1	1.3×10^{-3}	2.7	1.2×10^{-2}	2.
5.2×10^{-2}	5.6×10^{-3}	2.1	1.8×10^{-4}	2.9	2.1×10^{-3}	2.6
2.6×10^{-2}	1.4×10^{-3}	2.	2.3×10^{-5}	3.	4.1×10^{-4}	2.4
1.3×10^{-2}	3.4×10^{-4}	2.	2.9×10^{-6}	3.	$1. \times 10^{-4}$	2.

h	$\ \mathbf{u}_h \cdot \mathbf{n}\ _{\mathbb{L}^2}$	Order	Outer iterations	Residual norm
8.33×10^{-1}	3.4×10^{-1}		25	5.1×10^{-9}
4.17×10^{-1}	5.3×10^{-2}	2.7	33	3.3×10^{-9}
2.08×10^{-1}	4.9×10^{-3}	3.4	32	$1. \times 10^{-8}$
1.04×10^{-1}	$5. \times 10^{-4}$	3.3	29	8.3×10^{-9}
5.21×10^{-2}	4.9×10^{-5}	3.4	27	4.7×10^{-9}
2.6×10^{-2}	$5. \times 10^{-6}$	3.3	26	5.1×10^{-9}
1.3×10^{-2}	5.9×10^{-7}	3.1	34	8.5×10^{-9}

Table 7: Convergence results. $\tau = h^{-2}$, $\rho_u = h^{-1}$, $\rho_p = h^{-1}$, $\mathbf{C}_\star = \mathbf{C}_n$. Matrices are assembled as in (29)–(30)

$m \in \mathbf{m}_{1/2}$ as in Figure 5						
h	$\ \mathbf{u} - \mathbf{u}_h\ _{\mathbb{H}^1}$	Order	$\ \mathbf{u} - \mathbf{u}_h\ _{\mathbb{L}^2}$	Order	$\ p - p_h\ _{\mathbb{L}^2}$	Order
8.3×10^{-1}	1.3		5.2×10^{-1}		5.6×10^{-1}	
4.2×10^{-1}	$4. \times 10^{-1}$	1.7	8.7×10^{-2}	2.6	$2. \times 10^{-1}$	1.5
2.1×10^{-1}	1.3×10^{-1}	1.6	2.1×10^{-2}	2.1	1.2×10^{-1}	7.6×10^{-1}
$1. \times 10^{-1}$	5.2×10^{-2}	1.3	7.5×10^{-3}	1.5	6.4×10^{-2}	9.1×10^{-1}
5.2×10^{-2}	$2. \times 10^{-2}$	1.4	2.6×10^{-3}	1.5	2.6×10^{-2}	1.3
2.6×10^{-2}	6.3×10^{-3}	1.7	7.7×10^{-4}	1.7	8.5×10^{-3}	1.6
1.3×10^{-2}	1.8×10^{-3}	1.8	2.1×10^{-4}	1.9	2.4×10^{-3}	1.8

h	$\ \mathbf{u}_h \cdot \mathbf{n}\ _{\mathbb{L}^2}$	Order	Outer iterations	Residual norm
8.33×10^{-1}	3.4×10^{-1}		25	3.1×10^{-9}
4.17×10^{-1}	5.3×10^{-2}	2.7	31	5.5×10^{-9}
2.08×10^{-1}	4.9×10^{-3}	3.4	33	4.4×10^{-9}
1.04×10^{-1}	$5. \times 10^{-4}$	3.3	31	$1. \times 10^{-8}$
5.21×10^{-2}	4.9×10^{-5}	3.4	31	3.7×10^{-9}
2.6×10^{-2}	$5. \times 10^{-6}$	3.3	28	9.8×10^{-9}
1.3×10^{-2}	5.9×10^{-7}	3.1	34	9.6×10^{-9}

4 Inf-sup stability: pressure Schur complement generalized eigenvalues

4.1 Solution description. We define matrices

$$\mathbf{C}_0 := \mathbf{0}, \quad \mathbf{M}_n := \mathbf{M}_0 + \mathbf{C}_n, \quad \mathbf{M}_{\text{full}} := \mathbf{M}_0 + \mathbf{C}_{\text{full}}. \quad (31)$$

We are interested in (generalized) extreme eigenvalues of the pressure Schur complement matrices

$$\mathbf{S}_0 := \mathbf{B} \mathbf{A}^{-1} \mathbf{B}^T, \quad \mathbf{S}_n := \mathbf{S}_0 + \mathbf{C}_n, \quad \mathbf{S}_{\text{full}} := \mathbf{S}_0 + \mathbf{C}_{\text{full}}, \quad (32)$$

i.e. in solving

$$\mathbf{S}_\star \mathbf{x} = \lambda \mathbf{M}_\star \mathbf{x}, \quad (33)$$

where “ \star ” stands for “0,” “ n ,” or “full.” We denote by $0 = \lambda_1 < \lambda_2 \leq \dots \leq \lambda_{n_s} = O(1)$ the spectrum of (33).

Computing \mathbf{A}^{-1} in (32) becomes troublesome already for $h = 5.21 \times 10^{-2}$ ($n_A = 32736$ for $\mathbf{u} \in \mathbf{P}_1$ FE space): although \mathbf{A} is sparse, \mathbf{A}^{-1} is dense and consumes 8.5+ GB in double-precision arithmetic. A quick research showed that **Mathematica** has no built-in matrix-free eigenvalue routines. **Intel MKL**’s FEAST algorithm for computing (generalized) eigenvalues in an interval is suitable for matrix-free implementations; however, it requires some expensive operations to be implemented (e.g. matrix-matrix multiplications $\mathbf{Y} \leftarrow \mathbf{S}_\star \mathbf{X}$, $\mathbf{Y} \leftarrow \mathbf{M}_\star \mathbf{X}$ and approximating the action of inverses in the form $\mathbf{y} \leftarrow (\sigma \mathbf{M}_\star - \mathbf{S}_\star)^{-1} \mathbf{x}$).

Taking this into account, instead of (33) we consider a perturbed² problem

$$\underbrace{\begin{bmatrix} \mathbf{A} & \mathbf{B}^T \\ \mathbf{B} & -\mathbf{C}_\star \end{bmatrix} \begin{bmatrix} \mathbf{x} \\ \mathbf{y} \end{bmatrix}}_{\mathcal{A}_\star :=} = \mu \underbrace{\begin{bmatrix} \epsilon \mathbf{A} & \\ & \mathbf{M}_\star \end{bmatrix} \begin{bmatrix} \mathbf{x} \\ \mathbf{y} \end{bmatrix}}_{\mathcal{M}_\star^\epsilon :=} \quad (34)$$

with $0 < \epsilon \ll 1$. For \mathcal{A}_0 and \mathcal{M}_0^ϵ we have

$$\mu = -\lambda + o(1) \quad \text{or} \quad \epsilon^{-1} + \lambda + o(1), \quad \epsilon \rightarrow 0. \quad (35)$$

This makes it easy to pick only “correct” eigenvalues. To ease the computation further we replace the $(1, 1)$ -block of $\mathcal{M}_\star^\epsilon$ with $\epsilon \mathbf{I}$.

To make sure that results are consistent we solve (34) for $\epsilon = 10^{-5}$ and $\epsilon = 10^{-6}$; for the coarse mesh levels we also check that the dense solver for (33) and the iterative one for (34) give solutions that coincide in finite precision. See Table 8.

Table 8: Eigenvalues differences: dense solver for (33) and the iterative solver for (34). Corresponding eigenvalues are denoted as $\{\lambda_i\}$ and $\{\lambda_i^\mu\}$. Results are shown for consistent $\mathbf{P}_2 - P_1$, $\tau = h^{-2}$, $\rho_u = h^{-1}$, $\rho_p = h$, $m \in \mathbf{m}_{1/2}$ as in Figure 5

h	$\Gamma = \Gamma_{\text{sph}}$					
	\mathbf{S}_0		\mathbf{S}_n		\mathbf{S}_{full}	
	$ \lambda_2 - \lambda_2^\mu $	$ \lambda_{n_s} - \lambda_{n_s}^\mu $	$ \lambda_2 - \lambda_2^\mu $	$ \lambda_{n_s} - \lambda_{n_s}^\mu $	$ \lambda_2 - \lambda_2^\mu $	$ \lambda_{n_s} - \lambda_{n_s}^\mu $
8.33×10^{-1}	1.22×10^{-7}	5.97×10^{-6}	4.28×10^{-7}	2.09×10^{-7}	1.05×10^{-6}	1.5×10^{-7}
4.17×10^{-1}	5.14×10^{-9}	1.2×10^{-5}	8.74×10^{-7}	4.72×10^{-6}	9.25×10^{-6}	3.06×10^{-6}
2.08×10^{-1}	1.06×10^{-8}	4.15×10^{-5}	1.05×10^{-6}	4.34×10^{-5}	7.1×10^{-6}	2.8×10^{-5}

4.2 Dependency of the spectrum on the mesh size. Here we test inconsistent $\mathbf{P}_1 - P_1$ and consistent $\mathbf{P}_2 - P_1$ approaches.

²The majority of generalized eigenvalue solvers require left-hand-side matrix to be Hermitian and right-hand-side matrix to be Hermitian **positive definite**; that’s why we need to introduce $\epsilon > 0$.

Table 9: Spectrum of (33) for inconsistent $\mathbf{P}_1 - P_1$, $\tau = h^{-2}$, $\rho_u = h$, $\rho_p = h$, $m \equiv 2$

$\Gamma = \Gamma_{\text{sph}}$								
h	$n_{\mathbf{A}}$	$n_{\mathbf{S}}$	\mathbf{S}_0		\mathbf{S}_n		\mathbf{S}_{full}	
			λ_2	$\lambda_{n_{\mathbf{S}}}$	λ_2	$\lambda_{n_{\mathbf{S}}}$	λ_2	$\lambda_{n_{\mathbf{S}}}$
8.33×10^{-1}	153	51	1.32×10^{-2}	1.42	7.48×10^{-1}	1.13	9.58×10^{-1}	1.06
4.17×10^{-1}	570	190	5.12×10^{-3}	1.04	5.77×10^{-1}	1.	8.54×10^{-1}	1.
2.08×10^{-1}	1992	664	4.4×10^{-3}	7.93×10^{-1}	3.87×10^{-1}	1.	6.71×10^{-1}	1.
1.04×10^{-1}	8292	2764	2.01×10^{-3}	7.79×10^{-1}	2.19×10^{-1}	1.	5.82×10^{-1}	1.
5.21×10^{-2}	32736	10912	6.04×10^{-5}	9.81×10^{-1}	1.17×10^{-1}	1.	5.37×10^{-1}	1.
2.6×10^{-2}	131592	43864	3.53×10^{-5}	8.67×10^{-1}	5.72×10^{-2}	1.	5.16×10^{-1}	1.
1.3×10^{-2}	525864	175288	2.16×10^{-6}	7.34×10^{-1}	2.84×10^{-2}	1.	5.04×10^{-1}	1.

$\Gamma = \Gamma_{\text{tor}}$								
h	$n_{\mathbf{A}}$	$n_{\mathbf{S}}$	\mathbf{S}_0		\mathbf{S}_n		\mathbf{S}_{full}	
			λ_2	$\lambda_{n_{\mathbf{S}}}$	λ_2	$\lambda_{n_{\mathbf{S}}}$	λ_2	$\lambda_{n_{\mathbf{S}}}$
2.08×10^{-1}	972	324	5.04×10^{-2}	4.93	2.84×10^{-1}	1.35	3.64×10^{-1}	1.19
1.04×10^{-1}	4740	1580	2.99×10^{-3}	3.83	1.58×10^{-1}	1.02	3.35×10^{-1}	1.01
5.21×10^{-2}	19704	6568	1.11×10^{-3}	5.45	7.73×10^{-2}	1.01	3.25×10^{-1}	1.
2.6×10^{-2}	80808	26936	1.2×10^{-4}	5.42	3.07×10^{-2}	1.01	3.21×10^{-1}	1.
1.3×10^{-2}	327036	109012	1.77×10^{-5}	5.23	1.18×10^{-2}	1.01	3.16×10^{-1}	1.

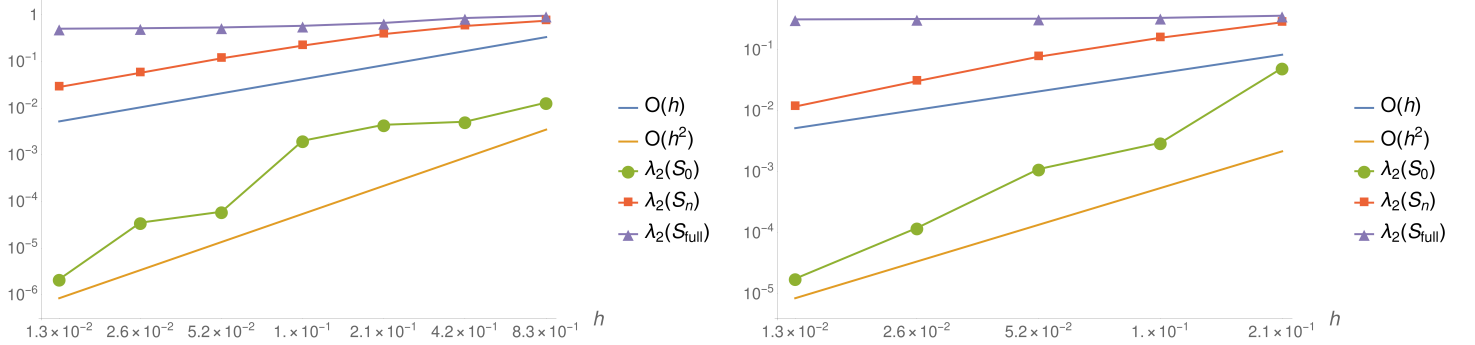


Figure 6: Log-log plot of λ_2 for Table 9. Left: $\Gamma = \Gamma_{\text{sph}}$, right: $\Gamma = \Gamma_{\text{tor}}$

Table 10: Spectrum of (33) for consistent $\mathbf{P}_2 - P_1$, $\tau = h^{-2}$, $\rho_u = h^{-1}$, $\rho_p = h$, $m \in \mathbf{m}_{1/2}$ as in Figure 5

$\Gamma = \Gamma_{\text{sph}}$								
h	$n_{\mathbf{A}}$	$n_{\mathbf{S}}$	\mathbf{S}_0		\mathbf{S}_n		\mathbf{S}_{full}	
			λ_2	$\lambda_{n_{\mathbf{S}}}$	λ_2	$\lambda_{n_{\mathbf{S}}}$	λ_2	$\lambda_{n_{\mathbf{S}}}$
8.33×10^{-1}	789	51	2.33×10^{-1}	1.07	6.3×10^{-1}	1.	8.81×10^{-1}	1.
4.17×10^{-1}	3276	190	4.72×10^{-2}	6.97×10^{-1}	5.29×10^{-1}	1.	7.64×10^{-1}	1.
2.08×10^{-1}	11718	664	7.93×10^{-2}	6.7×10^{-1}	5.09×10^{-1}	1.	6.39×10^{-1}	1.
1.04×10^{-1}	48762	2764	3.71×10^{-2}	6.69×10^{-1}	5.03×10^{-1}	1.	5.73×10^{-1}	1.
5.21×10^{-2}	193086	10912	1.81×10^{-3}	6.68×10^{-1}	4.98×10^{-1}	1.	5.36×10^{-1}	1.
2.6×10^{-2}	775998	43864	6.65×10^{-4}	6.65×10^{-1}	4.92×10^{-1}	1.	5.17×10^{-1}	1.

$\Gamma = \Gamma_{\text{tor}}$								
h	$n_{\mathbf{A}}$	$n_{\mathbf{S}}$	\mathbf{S}_0		\mathbf{S}_n		\mathbf{S}_{full}	
			λ_2	$\lambda_{n_{\mathbf{S}}}$	λ_2	$\lambda_{n_{\mathbf{S}}}$	λ_2	$\lambda_{n_{\mathbf{S}}}$
2.08×10^{-1}	5580	324	2.15×10^{-1}	9.56×10^{-1}	3.12×10^{-1}	1.	3.4×10^{-1}	1.
1.04×10^{-1}	28116	1580	1.59×10^{-2}	7.6×10^{-1}	3.21×10^{-1}	1.	3.35×10^{-1}	1.
5.21×10^{-2}	116592	6568	1.31×10^{-3}	7.48×10^{-1}	3.21×10^{-1}	1.	3.26×10^{-1}	1.
2.6×10^{-2}	477708	26936	1.9×10^{-4}	7.42×10^{-1}	3.2×10^{-1}	1.	3.22×10^{-1}	1.

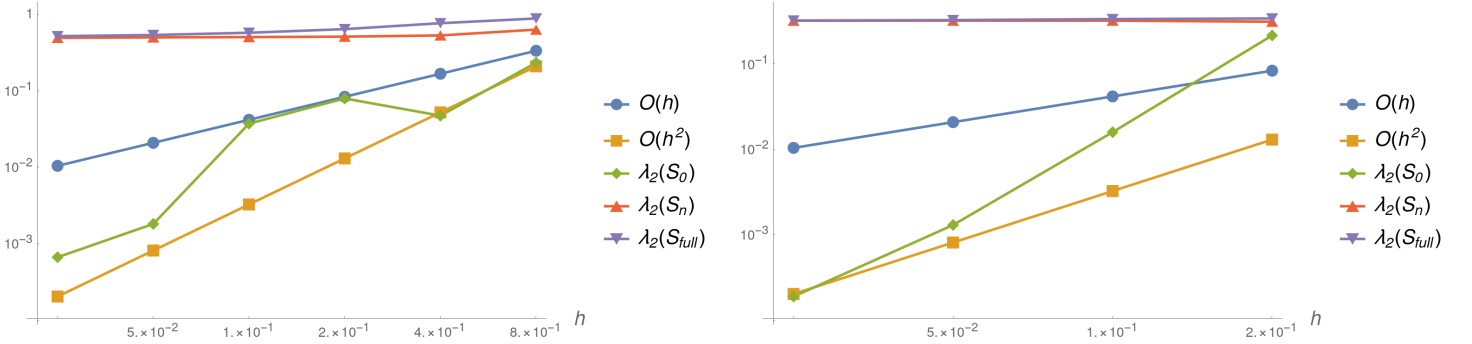


Figure 7: Log-log plot of λ_2 for Table 10. Left: $\Gamma = \Gamma_{\text{sph}}$, right: $\Gamma = \Gamma_{\text{tor}}$

4.3 Sensitivity of the spectrum to levelset shifts. In this section we investigate the sensitivity of the spectrum to levelset shifts

$$\Gamma \mapsto \Gamma + \alpha \mathbf{s} \quad (36)$$

for some $\alpha \in \mathbb{R}$ and $\mathbf{s} \in \mathbb{R}^3$, $\|\mathbf{s}\| = 1$. We refer to Figure 8.

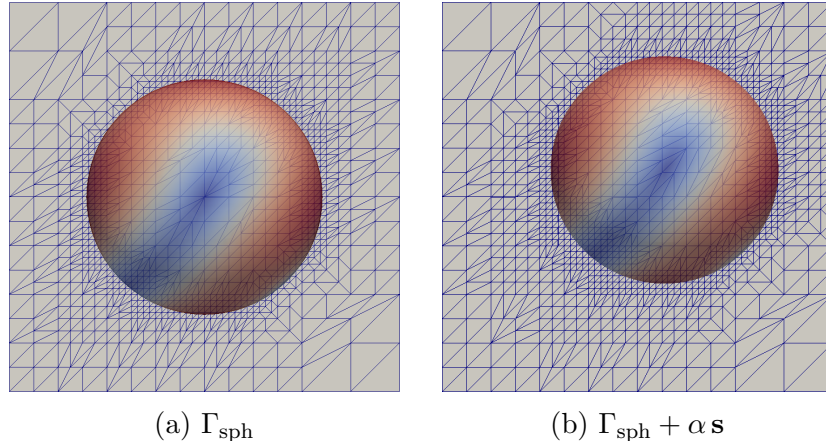


Figure 8: $\|\mathbf{u}_h\|$ on the unit sphere (left) and the shifted unit sphere (right). Here $\mathbf{s} = (1, 1, 1)^T / \sqrt{3}$, $\alpha = 0.4$, and $h = 5.21 \times 10^{-2}$

Table 11: Spectrum of (33) for perturbed levelset $\Gamma + \alpha \mathbf{s}$ for consistent $\mathbf{P}_2 - P_1$, $\tau = h^{-2}$, $\rho_u = h^{-1}$, $\rho_p = h$, $m \in \mathbf{m}_{1/2}$ as in Figure 5. Here $\mathbf{s} = (1, 1, 1)^T / \sqrt{3}$, $h = 1.04 \times 10^{-1}$

Surface	\mathbf{S}_0		\mathbf{S}_n		\mathbf{S}_{full}	
	λ_2	λ_{ns}	λ_2	λ_{ns}	λ_2	λ_{ns}
$\Gamma_{\text{sph}} + 0.0 \mathbf{s}$	3.714×10^{-2}	6.69×10^{-1}	5.03×10^{-1}	1.	5.731×10^{-1}	1.
$\Gamma_{\text{sph}} + 0.1 \mathbf{s}$	1.313×10^{-3}	6.87×10^{-1}	5.03×10^{-1}	1.	5.733×10^{-1}	1.
$\Gamma_{\text{sph}} + 0.2 \mathbf{s}$	1.248×10^{-3}	6.7×10^{-1}	5.03×10^{-1}	1.	5.73×10^{-1}	1.
$\Gamma_{\text{sph}} + 0.3 \mathbf{s}$	1.036×10^{-2}	6.72×10^{-1}	5.031×10^{-1}	1.	5.73×10^{-1}	1.
$\Gamma_{\text{sph}} + 0.4 \mathbf{s}$	5.315×10^{-4}	6.72×10^{-1}	5.031×10^{-1}	1.	5.731×10^{-1}	1.

Surface	\mathbf{S}_0		\mathbf{S}_n		\mathbf{S}_{full}	
	λ_2	λ_{ns}	λ_2	λ_{ns}	λ_2	λ_{ns}
$\Gamma_{\text{tor}} + 0.00 \mathbf{s}$	1.591×10^{-2}	7.6×10^{-1}	3.208×10^{-1}	1.	3.348×10^{-1}	1.
$\Gamma_{\text{tor}} + 0.05 \mathbf{s}$	9.204×10^{-3}	1.14	3.207×10^{-1}	1.	3.353×10^{-1}	1.
$\Gamma_{\text{tor}} + 0.10 \mathbf{s}$	$3. \times 10^{-3}$	1.91	3.189×10^{-1}	1.	3.349×10^{-1}	1.
$\Gamma_{\text{tor}} + 0.15 \mathbf{s}$	8.67×10^{-3}	1.02	3.208×10^{-1}	1.	3.354×10^{-1}	1.
$\Gamma_{\text{tor}} + 0.20 \mathbf{s}$	6.683×10^{-3}	3.04	3.208×10^{-1}	1.	3.353×10^{-1}	1.

5 Notes on DROPS implementation

5.1 VTK output. DROPS implements its own routines for writing *.vtu files (for Paraview or Visit to read). What I noticed is that they take a lot of space for finer mesh levels, even if one uses binary output format. This is a bottleneck when one wants to generate the output for transient problems.

What I did is, I implemented another class for writing *.vtu files, cf. [here](#). The difference from the old implementation is that this new class utilizes the official [VTK library](#), i.e. it does not implement writing of *.vtu from scratch.

The two implementations are compared via exporting the following data: Mesh nodes (including middle points of edges) and element connectivity, level-set scalar field $I_h(\phi)$, 2 pressure scalar fields $I_h(p)$ and p_h , and 2 vector fields $I_h(\mathbf{u})$ and \mathbf{u}_h .

Table 12: ASCII output

h	CPU time, seconds		Size of *.vtu	
	Old implementation	New implementation	Old implementation	New implementation
2.08×10^{-1}	0.123	0.0874	1.3 M	2.3 M
1.04×10^{-1}	0.314	0.158	4.9 M	8.8 M
5.21×10^{-2}	1.189	0.495	21 M	37 M

Table 13: Binary output

h	CPU time, seconds		Size of *.vtu	
	Old implementation	New implementation	Old implementation	New implementation
2.08×10^{-1}	0.0919	0.107	1.1 M	540 K
1.04×10^{-1}	0.202	0.219	4.2 M	2.2 M
5.21×10^{-2}	0.755	0.781	19 M	9 M

From Table 13 we see that the CPU time for both implementations are comparable, and the new implementation is twice as efficient in terms of the space usage. Which is nice.

Note: From Table 12 we see that the new implementation produces twice as large files in ASCII format. This is simply because we write the fields in double precision, and the old implementation writes numbers in single precision (i.e. each text representation of a number is 16 characters against 8). Anyway, this does not matter, for in practice we are using binary format.

References

- [1] Michele Benzi and Maxim A Olshanskii. An augmented lagrangian-based approach to the oseen problem. *SIAM Journal on Scientific Computing*, 28(6):2095–2113, 2006.
- [2] T. Jankuhn and A. Reusken. Trace Finite Element Methods for Surface Vector-Laplace Equations. *arXiv e-prints*, April 2019.
- [3] Thomas Jankuhn, Maxim Olshanskii, and Arnold Reusken. Incompressible fluid problems on embedded surfaces: Modeling and variational formulations. *Interfaces and Free Boundaries*, 20(3):353377, Nov 2018.
- [4] M. Olshanskii, A. Quaini, A. Reusken, and V. Yushutin. A finite element method for the surface stokes problem. *SIAM Journal on Scientific Computing*, 40(4):A2492–A2518, 2018.